CrystEngComm

Accepted Manuscript

ROYAL SOCIETY OF CHEMISTRY

www.rsc.org/crystengcomm

An effective route to the synthesis of boron nitride micro-nano structure and the growth mechanism

An Pan[1, 2], Yongjun Chen[1,*], Jianbao Li[1]

[1] Key Lab of Advanced Materials of Tropical Island Resources, Ministry of Education, College of Materials and Chemical Engineering, Hainan University, Haikou 570228, China

[2] College of Chemistry & Chemical Engineering, Guangxi University, Nanning 530004, China

* The corresponding author. Email: chenyj99@163.com (Y. J. Chen)

Abstract An efficient route to the large scale synthesis of boron nitride (BN) micro-nano structure called nanosheet-assembled microwires is demonstrated for the first time, by annealing amorphous boron powders with ferric chloride ($FeCl_3$) at elevated temperatures in flowing ammonia atmosphere. The microwires have a very well-proportioned diameter of about 2 μm, while the nanosheets have an average thickness of less than 20 nm. The nanosheets are mostly separated with a bending and crumpling morphology and nearly vertically aligned to the microwire trunk. This micro-nano structure shows strong photoluminescence (PL) emission at 357 nm. It is revealed that $FeCl_3$ reacts with B to generate BCl_3, a vital vapor for the growth of BN micro-nano structures in addition to the provision of catalyst Fe. A combination growth mechanism of vapor-liquid-solid (VLS) and vapor-solid (VS) model is proposed to be responsible for the formation of this BN micro-nano structure.

1. Introduction

The discovery of graphene has fascinated the science community and enthused a great deal of interests in developing two-dimensional (2D) nanostructures on account of their remarkable properties such as superb mechanical properties, sharp open edges and extraordinary room-temperature carrier mobility.[1-4] Hexagonal boron nitride (*h*-BN) is an isoelectric analog of graphite, but possesses a larger band gap (nearly 6 eV) and enhanced chemical stability in comparison with graphite in addition to the wonderful mechanical strength and high thermal conductivity.[5,6] One-dimensional (1D) BN nanotubes (BNNTs) have been considerably studied.[7-9] However, 2D BN nanosheets (BNNSs) have rarely been reported. BNNSs were reported to display strong oxidation resistance,[10] high surface area,[11] strong cathodoluminescence emission[12-14] and outstanding superhydrophobicity with self-cleaning ability,[12,15] indicating extremely promising application in the fields of hydrogen storage, gas detection, electron emission, light-emitting diodes and so on. Thus, it is of great significance to synthesize BNNSs in a simple but efficient way. To date, several approaches are available to prepare few-layered BNNSs, including micromechanical cleavage method,[16,17] ball-milling peeling method,[18] chemical-solution-derived method[19-22] and other method.[23] Chemical vapor deposition (CVD) method is also an important technique to synthesize BNNSs.[24-26] However, the greatest disadvantage of these methods is the low production and or low purity of BNNSs, which would limit the application of BNNSs.

In addition, BN micro-nano structures were reported to exhibit some appealing properties and have potential applications in lasing, field-emission displays, composite materials and nanodevices.[8,27-30] However, BN nanosheet-assembled microwires especially in large quantity and with high purity, has not been reported so far. Herein, we reported a simple but efficient route to the mass-production of BN micro-nano structure called nanosheet-assembled microwires, by simply annealing amorphous B powders with catalyst $FeCl_3$ in NH_3 atmosphere. $FeCl_3$ has been reported as catalyst for successfully synthesizing BN nanowires before, which proved

its catalytic effectiveness for the growth of BN material.[31] The BN micro-nano structure we prepared was quite pure and uniform. The effect of synthetic temperature on the formation of the structure was discussed. Combined with structural characterizations, possible growth mechanism for the formation of this BN micro-nano structures was proposed. In addition, the photoluminescence (PL) property of the BN micro-nano structures was investigated.

2. Experimental

In a typical procedure, amorphous B powders (98% purity) and $FeCl_3 \cdot 6H_2O$ with a molar ratio of 1: 0.05 were selected as the raw materials. Firstly, $FeCl_3 \cdot 6H_2O$ was dissolved in absolute ethyl alcohol, then B powders were added into the solution. The mixture was stirred and heated in a water bath at 40 ºC for 2 h, followed by being dried at 55 ^{o}C to thoroughly remove the solvent. After that, a homogeneous precursor was obtained. The precursor was loaded into an alumina boat which was placed at the center of a tubular furnace. Before heating up, high-purity NH_3 flow (1000 $mLmin^{-1}$) was introduced to flush out the residual air in the chamber. Then the furnace was heated to 1200 ºC at a rate of 10 ºCmin^{-1} under NH_3 flow (50 $mLmin^{-1}$) and held for 5 h. Finally, the furnace was cooled naturally to ambient temperature under the protection of N_2 flow.

Afterwards, a large quantity of white product was obtained in the boat. The product was collected and characterized by scanning electron microscopy (SEM, Zeiss Merlin), transmission electron microscopy (TEM), high-resolution TEM (HRTEM, JEOL JEM-2011) equipped with X-ray energy dispersive spectrometer (EDS) and electron energy loss spectroscopy (EELS, FEI Titan 80-300). The PL property of the BN micro-nano structures was measured at room temperature (Edinburgh FLS920, 300 nm excitation).

3. Results and discussion

3.1. Morphology, microstructure and composition of the as-synthesized products

Fig. 1 shows the digital photo of the as-synthesized white product, indicating a high-ratio nitriding reaction of the raw materials. Fig. 2 shows the SEM images of the product. It can be seen that the product consists of large quantity of 1D structures with length up to hundreds microns (Fig. 2a). Nearly no particles can be found in the product. The enlarged SEM image (Fig. 2b) reveals that the 1D structures are composed of a micro-nano structure, namely microwires made by assembly of nanosheets. The microwires have relatively uniform diameters with a typical value of about 2 μm. Further enlarged image (Fig. 2c) illustrates much clearly that the thin nanosheets are mostly separated with a bending and crumpling morphology and nearly vertically aligned to the trunk. Due to the edge bending of the nanosheets, it is difficult to accurately determine their thickness from the SEM image. For most of the nanosheets, the thickness could be roughly measured to be less than 20 nm. Interestingly, branched nanosheets are observed, that is, subnanosheets grow on the surface of the main nanosheets, forming three-dimensional nanostructures. It was believed that the branching BNNSs have the advantage of preventing conglomeration and thus are able to preserve their high surface area.[13] Fig. 2d demonstrates the cross-section of a microwire, revealing the radial growth direction of the nanosheets. Moreover, a nanosized 'solid' core can be seen (as shown by the white arrow), which may be a suspected bamboo-like nanotube that happens to be broken in the compartment part and will be verified later in this study.

Fig. 3 shows the TEM images of micro-nano structures. It can be seen that the nanosheets are thin and vertically separated, which is consistent with the SEM observation (Fig.3 a). From Fig. 3b, it is clearly observed that the nanosheets are bending and scrolling with taped edge morphology, which is anticipated as an intrinsic property of 2D nanostructures and similar to those found in BNNSs and carbon nanosheets (CNSs).[13,32] Fig. 3c is the HRTEM image showing the rectangle region in Fig. 3b, highly ordered lattice fringes can be clearly observed. The interlayer spacing between adjacent fringes is about 0.334 nm, corresponding to the (002) planes of h-BN. The transparency of the nanosheets to the electron beam displays its ultrathin nature, as is demonstrated clearly in Fig. 3d and the inset. Moreover, few

layers (2-5 layers) of a nanosheet edge can be counted due to the crumpling and folding of the nanosheet.[26,32] The interlayer spacing of about 0.331 nm reveals the crystalline perfection of the *h*-BN nanosheets.

EDS result is acquired from a microwire and shown in Fig. 4a, showing the dominating peaks of B, N, and Cu with a small amount of O, Fe and Cr. The Cu peaks can be ascribed to the copper TEM grid, while the slight O signal should be attributed to slight surface oxidation or oxygen adsorption due to the high reaction activity of micro-nano structure.[13,33] The weak Fe peak could be induced by the inclusion of catalyst $FeCl_3$. While the Cr signal is probably from the impurity in the raw materials. Hence, the micro-nano structures are verified to be composed of BN again. The chemical composition and stoichiometric proportion of the micro-nano structure are further proved by means of EELS technique. Fig. 4b depicts a typical EELS spectrum of a nanosheet that having two pronounced adsorption peaks of B and N characteristic K-edges at 188 and 401 eV, respectively. The sharp peaks on the left side and the broad peaks on the right side of adsorption features correspond to π^* and σ^* anti-bonding orbits, respectively, which are representative features of an sp^2-hybrizied state. The relative quantification analysis offers a B/N atomic ratio of 0.97. Therefore, it can be concluded that the synthesized product are BN nanosheet-assembled microwires.

3.2. Photoluminescence property of as-synthesized BN micro-nano structures

Fig. 5 shows the room-temperature PL property of the product. The spectrum displays three main emission bands centered at 357, 673 and 735 nm. Normally, the possibility of a material to demonstrate luminescence relies on the intrinsic band edge structure and other internal or external factors (intrinsic/ extrinsic defects).[34,35] Some emission peaks in the range 300-400 nm have been reported that they mainly originate from residual impurities such as carbon and oxygen[36-39] and partially from O_2 adsorption.[40] Therefore, the luminescence band at about 357 nm can be mainly assigned to the oxygen impurity (as is detected by EDS). Chen et al. interpreted 680 nm PL emission in periodic yard-glass shaped BN nanotubes that it might be ascribed to lattice defects

in the structures and their inserting connection mode.[37] In addition, it was discovered that emission band at 700 nm of BN whiskers might originate from defect-trapped states (vacancy-type defect) and a quantum confinement effect.[41] Long-wavelength emissions at 728 and 703 nm were also found in BN nanowires and nanotubes in our previous studies due to the intrinsic lattice defects as well.[42,43] Hence, it is reasonable that emission bands located at around 673 and 735 nm in the current study are induced by intrinsic lattice defects related to the bending and crumpling morphologies or sharp open edges of the nanosheets.

3.3. Microstructure and composition of the BN micro-nano structures at earlier growth stage

Fig. 6a shows the SEM image of the product at the earlier growth stage. Smaller submicrometer wires (200-500 nm in diameter) made by assembly of numerous nanosheets can be observed. However, some structures with hollow core can also be found, as is shown by the white arrow. The enlarged image reveals the hollow core much clearly (the inset), which should be the caused by the break of a bamboo-shaped nanotube in the cavity part. TEM image (Fig. 6b) verifies that the core is a bamboo-like nanotube, which also confirms the former supposition with respect to Fig. 2d. The HRTEM image of a nanosheet (the inset) demonstrates well-defined lattice fringes with 0.331nm interlayer spacing, indicating the correspondence with (002) crystal planes of h-BN. EDS and EELS results (not shown here) of this structure also confirm the composition of BN. This result hints that the formation of the final BN nanosheet-assembled microwires may start from bamboo-shaped nanotubes.

3.4. The effect of temperature on the formation of BN micro-nano structures

To further understand the growth mechanism of the BN nanosheet-assembled microwires, the temperature effect was investigated. Fig. 7a and b shows the SEM images of the products synthesized at 1150 and 1250 ºC, respectively. The sample color obtained at 1150 ^{o}C is grey (the inset), implying an incomplete nitriding reaction of the boron powders. Moreover, smaller wires (ca. 1 micron) with lower yield are

produced. While the sample prepared at 1250 ºC looks nearly the same as that of 1200 ºC (the inset). However, the wires have a distinct increase in diameter (ca. 10 microns). Fig. 7c and d show the corresponding enlarged SEM images of the samples. A huge bulk of nanosheets can be seen to constitute the wires. However, the nanosheets grown at 1150 ºC are shorter and smaller than those grown at 1250 ºC.

3.5. The growth mechanism of BN micro-nano structures

Based on the results described above, two main growth stages relying on the generation and concentration of BCl_3 vapor that is related with the synthetic temperature could be accounted for the formation of this BN micro-nano structure, i.e., the nanotube growth stage at the initial of the process followed by the nanosheet growth and assembly stage. The possible reactions are elucidated as follow:

$$6FeCl_3\ (s) + 2NH_3\ (g) \rightarrow 6FeCl_2\ (s) + 6HCl\ (g) + N_2(g) \quad (1)$$

$\Delta G < 0$ (temperature in range of 0 ~ 1250 ^oC)

$$FeCl_2(s) \rightarrow FeCl_2\ (l) \quad (2)$$

$$FeCl_2\ (l) \rightarrow FeCl_2\ (g) \quad (3)$$

ΔG (1150, 1200, 1250 ^oC) = -14.820, -19.776, -24.670 kJ

$$3FeCl_2\ (g) + 2B\ (s) \rightarrow 2BCl_3\ (g) + 3Fe\ (l) \quad (4)$$

ΔG (1150, 1200, 1250 ^oC) = -44.265, -33.610, -22.991 kJ

$$3FeCl_2\ (l) + 2B\ (s) \rightarrow 2BCl_3\ (g) + 3Fe\ (l) \quad (5)$$

ΔG (1150, 1200, 1250 ^oC) = -88.726, -92.936, -97.000 kJ

$$BCl_3\ (g) + NH_3\ (g) \rightarrow BN\ (s) + 3HCl\ (g) \quad (6)$$

ΔG (1150, 1200, 1250 ^oC) = -216.077, -221.060, -226.045 kJ

Fig. 8 illustrates the schematic diagram of the formation of BN nanosheet-assembled microwires. At first, $FeCl_3$ is reduced to $FeCl_2$ (boiling point: 1023 ^oC) in ammonia atmosphere (equation 1). Along with heating up, $FeCl_2$ goes through a series of transformation from solid state to liquid and gas phase (equation 2 and 3). Thermodynamic calculations reveal that $FeCl_2$ reacts with B powder to generate BCl_3 vapor and the critical nucleation agent Fe droplets at synthetic

temperatures (equation 4 and 5). Fe droplets absorb the surrounding BCl_3 and NH_3 vapors to form a Fe-B-N alloy (step *a*). When the concentrations of the species in the droplets are greater than the saturation threshold, BN crystals begin to precipitate (equation 6 and step *a*). With the continuous provision of BCl_3 and NH_3 vapors, BN nanotubes are finally formed (step *b*), as is depicted in Fig. 6. The detailed formation process of bamboo-shaped nanotubes can be referred in previous studies.[44,45] And a vapor-liquid-solid (VLS) model is supposed to govern this growth stage. It should be noted here that Fe-containing catalyst particles are very hard to be found under electron microscopy, which may be due to the missing during the preparation process of TEM samples and the coverage of the nanosheet.

As for the second stage, i.e. the nanosheet growth on the already formed BN nanotubes, it has been reported that the surfaces of bamboo-shaped BN nanotubes are generally rough and have many defects that could serve as new nucleate sites for the further growth of BN crystals.[27,46] In addition, BN species have sufficiently high mobility at the synthetic temperatures. B and N atoms are absorbed to form new BN nuclei, which deposit on the surface of the nanotubes and then quickly diffuse from inside out to form the primary nanosheets (step *c*). The incoming BN species land on the surface of the growing nanosheets, rapidly move along the surface toward the edge of the nanosheets and covalently bond to the edge atoms before re-evaporated. While those BN species diffusing toward the nanotube instead of toward the growing edges can be re-evaporated due to the weak van der Waals forces attaching them to the nanotubes. Therefore, the nanosheets tend to grow higher rather than thicker. With the accumulation of sustaining BN species, the nanosheets keep growing radially while the bottom part becomes compact on account of the branching and thickening of the nanosheets. Finally, the BN nanosheet-assembled microwire is formed (step *d*). The whole process is very similar to those of CNSs and BNNSs.[12,13,47] In this process, BNNSs grow via the vapor-solid (VS) model.

It is interesting that both the nucleation agent Fe and BCl_3 vapor play important roles during the formation of this micro-nano structure. At 1200 ^{o}C, an appropriate amount of BCl_3 vapor and Fe droplets would be generated within the reaction

chamber, which lead to the large quantity formation of BN micro-nano structures. When the temperature lowers to 1150 ^{o}C, thermodynamic calculation indicates that the generation of BCl_3 vapor could still be realized, but the rate reduces. Moreover, the number of Fe liquid droplet decreases. The insufficiency of reactants (BCl_3 vapor) and catalyst (Fe) leads to the smaller size and lower yield of the micro-nano structures. The reactions occur at a much fast rate when the temperature increases to 1250 ^{o}C, which generate much more BCl_3 vapor within a short period of time. Some BCl_3 vapor will be flushed out of the chamber by NH_3 flow. At the same time, the number of Fe liquid droplets increases with the rise of temperature and larger catalyst droplets will form. As a result, thicker and lower yield of BN micro-nano structures are obtaiend.

4. Conclusions

A kind of BN micro-nano structure called nanosheet-assembled microwires is successfully synthesized in large quantity and with high purity by annealing $FeCl_3$ and amorphous B powders in NH_3 atmosphere. The diameters of the microwires are approximate 2 μm and thicknesses of the nanosheets are less than 20 nm. The generation and concentration of BCl_3 vapor, which depend on the experimental temperature, are vital for the formation of this micro-nano structure. Both yield and purity decrease at a lower temperature (i.e. 1150 ºC), while the diameters of the microwires increase tremendously at a higher temperature (i.e. 1250 ºC). A combined growth mechanism of VLS and VS model are proposed to govern the growth process of micro-nano structures. The structure possesses PL emissions at 357, 673 and 735 nm. This approach paves a new way with respect to BN micro-nano structures and their integrated utilization into modern technologies.

Acknowledgments

The project is supported by the National Science Foundation of China (Grants No. 51162001 and 51362008), Hainan University Scientific Research Funding (Grant No. kyqd1240) and Local

service project (Grant No. HDSF201308). The work makes use of the resources of the Beijing National Center for Electron Microscopy.

References

1 K. S. Novoselov, A. K. Geim, S. V. Morozov, D. Jiang, Y. Zhang, S. V. Dubonos, I. V. Grigorieva, A. A. Firsov, *Science*, 2004, **306**, 666.

2 I. W. Feank, D. M. Tanenbaum, A. M. van der Zande, P. L. McEuen, *J. Vac. Sci. Technol. B*, 2007, **25**, 2558.

3 N. G. Shang, P. Papakonstantinou, M. McMullan, M. Chu, A. Stamboulis, A. Potenza, S. S. Dhesi, H. Marchetto, *Adv. Funct. Mater*., 2008, **18**, 3506.

4 K. I. Bolotin, K. J. Sikes, Z. Jiang, M. Klima, G. Fudenberg, J. Hone, P. Kim, H. L. Stormer, *Solid State Commun*., 2008, **146**, 351.

5 D. Golberg, Y. Bando, Y. Huang, T. Terao, M. Mitome, C. C. Tang, C. Y. Zhi, *ACS Nano*, 2010, **4**, 2979.

6 A. Pakdel, C. Y. Zhi, Y. Bando, D. Golberg, *Mater. Today*, 2012, **15**, 256.

7 N. G. Chopra, R. J. Luyken, C. V. H. Crespi, M. L. Cohen, S. G. Louie, A. Zettl, *Science*, 1995, **269**, 966.

8 M. Bechelany, A. Brioude, S. Bernard, P. Stadelmann, D. Cornua, P. Mielea, *CrystEngComm*, 2011, **13**, 6526.

9 D. Golberg, Y. Bando, C. C. Tang, C. Y. Zhi, *Adv. Mater*. 2007, **19**, 2413.

10 L. H. Li, J. Cervenka, K. Watanabe, T. Taniguchi, Y. Chen, *ACS Nano*. 2014, **8**, 1457.

11 A. Nag, K. Raidongia, K. P. S. S. Hembram, R. Datta, U. V. Waghmare, C. N. R. Rao, *ACS Nano*, 2010, **4**, 1539.

12 A. Pakdel, C. Y. Zhi, Y. Bando, T. Nakayama, D. Golberg, *ACS Nano*, 2011, **5**, 6507.

13 J. Yu, L. Qin, Y. F. Hao, S. Y. Kuang, X. D. Bai, Y. M. Chong, W. J. Zhang, E. G. Wang, *ACS Nano*, 2010, **4**, 414.

14 A. Pierret, J. Loayza, B. Berini, A. Betz, B. Placais, F. Ducastelle, J. Barjon, A. Loiseau, *Phys. Rev. B*, 2014, **89**, 035414.

15 A. Pakdel, X. Wang, Y. Bando, D. Golberg, *Acta Mater*., 2013, **61**, 1266.

16 K. S. Novoselov, D. Jiang, F. Schedin, T. J. Booth, V. V. Khotkevich, S. V. Morozov, A. K. Geim, *Proc. Natl. Acad. Sci. USA*, 2005, **102**, 10451.

17 J. C. Meyer, A. Chuvilin, G. Algara-Siller, J. Biskupek, U. Kaiser, *Nano Lett*., 2009, **9**, 2683.

18 L. H. Li, Y. Chen, G. Behan, H. Z. Zhang, M. Petravic, A. M. Glushenkov, *J. Mater. Chem*., 2011, **32**, 11862.

19 W. Q. Han, L. Wu, Y. Zhu, K. Watanabe, T. Taniguchi, *Appl. Phys. Lett*., 2008, **93**, 223103.

20 Y. Lin, T. V. Williams, J. W. Connell, *J. Phys. Chem. Lett*. 2010, **1**, 277.

21 J. H. Warner, M. H. Rummeli, A. Bachmatiuk, B. Buchner, *ACS Nano*, 2010, **4**, 1299.

22 Y. Lin, T. V. Williams, T. B. Xu, W. Gao, H. E. Elsayed-Ali, J. W. Connell, *J. Phys. Chem. C*, 2011, **115,** 2679.

23 X. Zhang, G. Lian, S. J. Zhang, D. L. Cui, Q. L. Wang, *CrystEngComm*, 2012, **14**, 4670.

24 Y. Shi, C. Hamsen, X. Jia, K. K. Kim, A. Reina, M. Hofmann, A. L. Hsu, K. Zhang, H. Li, Z. Y. Juang, M. S. Dresselhaus, L. J. Li, J. Kong, *Nano Lett*., 2010, **10**, 4134.

25 K. H. Lee, H. J. Shin, J. Lee, I. Lee, G. H. Kim, J. Y. Choi, S. W. Kim, *Nano Lett*., 2012, **12**, 714.

26 S. Chatterjee, Z. Luo, M. Acerce, D. M. Yates, A. T. C. Johnson, L. G. Sneddon, *Chem. Mater*. 2011, **23**, 4414.

27 J. Li, H. Lin, Y. J. Chen, Q. Q. Su, X. F. Bi, *J. Alloys Compd*., 2013, **550**, 292.

28 H. Yu, X. Huang, G. Wen, T. Zhang, B. Zhong, H. Bai, *Mater. Chem. Phys*., 2011, **129**, 30.

29 Y. Zhu, Y. Bando, L. Yin, D. Golberg, *Nano Lett*., 2006, **6**, 2982.

30 Z. G. Chen, J. Zou, Q. Liu, C. Sun, G. Liu, X. Yao, F. Li, B. Wu, X. L. Yuan, T. Sekiguchi, H. M. Cheng, G. Q. Lu, *ACS Nano*, 2008, **2**, 1523.

31 K. F. Huo, Z. Hu, F. Chen, J. J. Fu, Y. Chen, B. H. Liu, J. Ding, Z. L. Dong, T. White, *Appl. Phys. Lett*., 2002, **80**, 3611.

32 J. C. Meyer, A. K. Geim, M. I. Katsnelson, K. S. Novoselov, T. J. Booth, S. Roth, *Nature*,

2007, **446**, 60.

33 M. Sajjad, P. Feng, *Mater. Res. Bull*., 2014, **49**, 35.

34 B. K. Gupta, V. Shanker, M. Arora, D. Haranath, *Appl. Phys. Lett*., 2009, **95**, 073115.

35 P. Jaffrennou, J. Barjon, J. S. Lauret, A. Maguer, D. Golberg, B. Attal-Tretout, F. Ducastelle, A. Loiseau, *Phys. Stat. Sol. B*, 2007, **244**, 4147.

36 P. Jaffrennou, J. Barjon, T. Schmid, L. Museur, A. Kaneav, J. S. Lauret, C. Y. Zhi, C. C. Tang, Y. Bando, D. Golberg, B. Attal-Tretout, F. Ducastelle, A. Loiseau, *Phys. Rev. B*, 2008, **77**, 235422.

37 Z. G. Chen, J. Zou, G. Liu, F. Li, H. M. Cheng, T. Sekiguchi, M. Gu, X. D. Yao, L. Z. Wang, G. Q. Lu, *Appl. Phys. Lett*., 2009, **94**, 023105.

38 T. Taniguchi, K. Watanabe, *J. Cryst. Growth*, 2007, **303**, 525.

39 L. H. Li, Y. Chen, B. M. Cheng, M. Y. Lin, S. L. Chou, Y. C. Peng, *Appl. Phys. Lett.*, 2012, **100**. 261108.

40 L. H. Li, Y. Chen, M. Y. Lin, A. M. Glushenkov, B. M. Cheng, H. Yu, *Appl. Phys. Lett.*, 2010, **97**, 141104.

41 Y. C. Zhu, Y. Bando, D. F. Xue, T. Sekiguchi, D. Golberg, F. F. Xu, Q. L. Liu, J. *Phys. Chem. B*, 2004, **108**, 6193.

42 Y. J. Chen, B. Chi, D. C. Mahon, Y. Chen, *Nanotechnology*, 2006, **17**, 2942.

43 J. Li, J. B. Li, Y. C. Yin, Y. J. Chen, X. F. Bi, *Nanotechnology*, 2013, **24**, 365605.

44 X. F. Bi, Y. C. Yin, J. B. Li, Y. J. Chen, J. Li, Q. Q. Su, *Solid State Sci*., 2013, **25**, 39.

45 L. B. Mo, Y. J. Chen, L. J. Luo, *Appl. Phys. A-Mater. Sci. Proc*., 2010, **100**, 129.

46 E. Bengu, L. D. Marks, *Phys. Rev. Lett*., 2001, **86**, 2385.

47 M. Zhu, J. Wang, B. C. Holloway, R. A. Outlaw, X. Zhao, K. Hou, V. Shutthanandan, D. M. Manos, *Carbon*, 2007, **45**, 2229.

Figure captions

Fig. 1 Digital photo of the as-synthesized white product.

Fig. 2 SEM images of the product. (a) Low-magnification image, showing one-dimensional (1D) structures with large quantity. (b) High-magnification image, demonstrating the nanosheet-assembled microwires. (c) Further magnified image, revealing the vertically aligned nanosheets with bending and crumpling morphology. (d) The cross-section image. The white arrow indicates a suspected bamboo-like nanotube core that happens to be broken in the compartment part, showing 'solid' nature.

Fig. 3 (a) TEM image of the nanosheet-assembled microwires. (b) TEM image of the edge part of the micro-nano structures, showing the bending and scrolling nanosheets with taped edge morphology. (c) HRTEM image of the rectangle region in b. (d) TEM image of the ultrathin nanosheets. The inset is the HRTEM image of the edge part of the nanosheet indicated by rectangle region, demonstrating the few layers of the nanosheet.

Fig. 4 (a) EDS result of a nanosheet-assembled microwire. (b) EELS spectrum of a nanosheet.

Fig. 5 (a) Photoluminescence property of the nanosheet-assembled microwires.

Fig. 6 Electron microscopy images of the product at the earlier growth stage. (a) SEM image, showing the smaller nanosheet-assembled submicrometer wires with diameters range from 200 to 500 nm. Two structures with hollow core are also found indicated by white arrow, which are demonstrated much clearly by the enlarged image shown in the inset. (b) TEM image of a nanosheet-assembled structure with bamboo-shaped nanotube core that is broken in the cavity part, showing a 'hollow' nature. The inset shows the HRTEM image of one nanosheet.

Fig. 7 Low-magnification SEM images of the product synthesized at (a) 1150 ºC and (b) 1250 ºC.

The insets are their corresponding digital photos. High-magnification SEM images of the product synthesized at (c) 1150 ºC and (d) 1250 ºC.

Fig. 8 The schematic diagram of the formation of a BN nanosheet-assembled microwire.

Figures

Fig. 1

Fig. 2

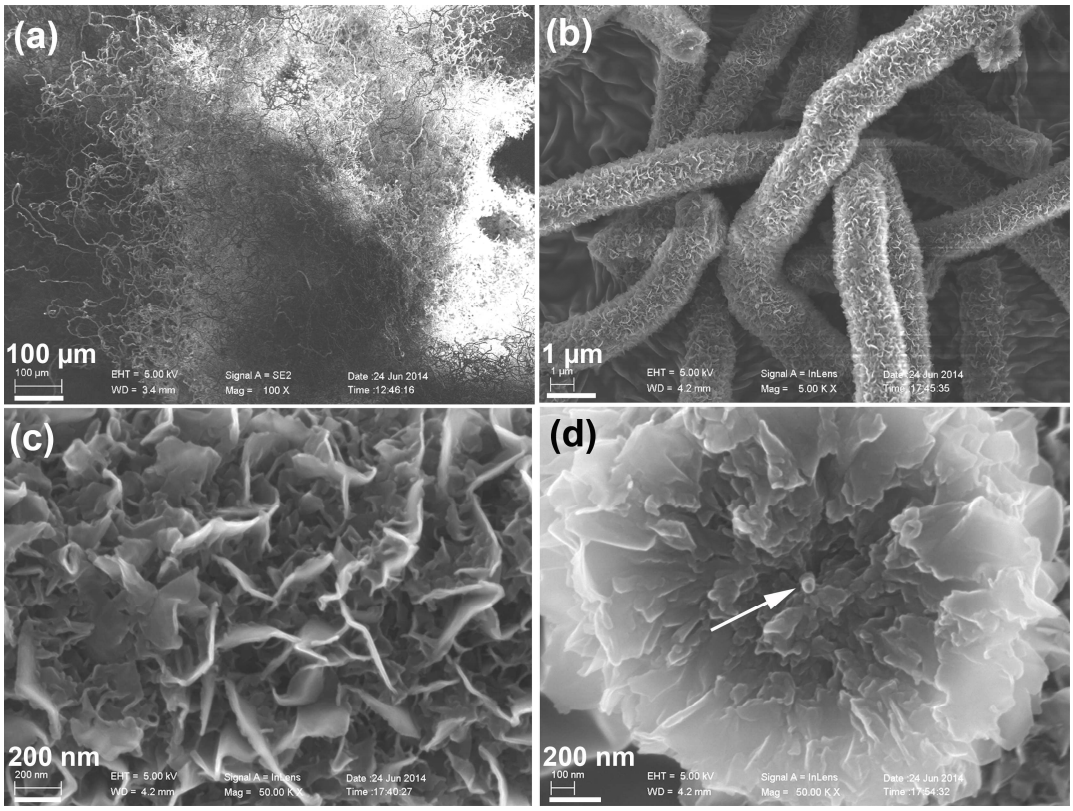

Fig. 3

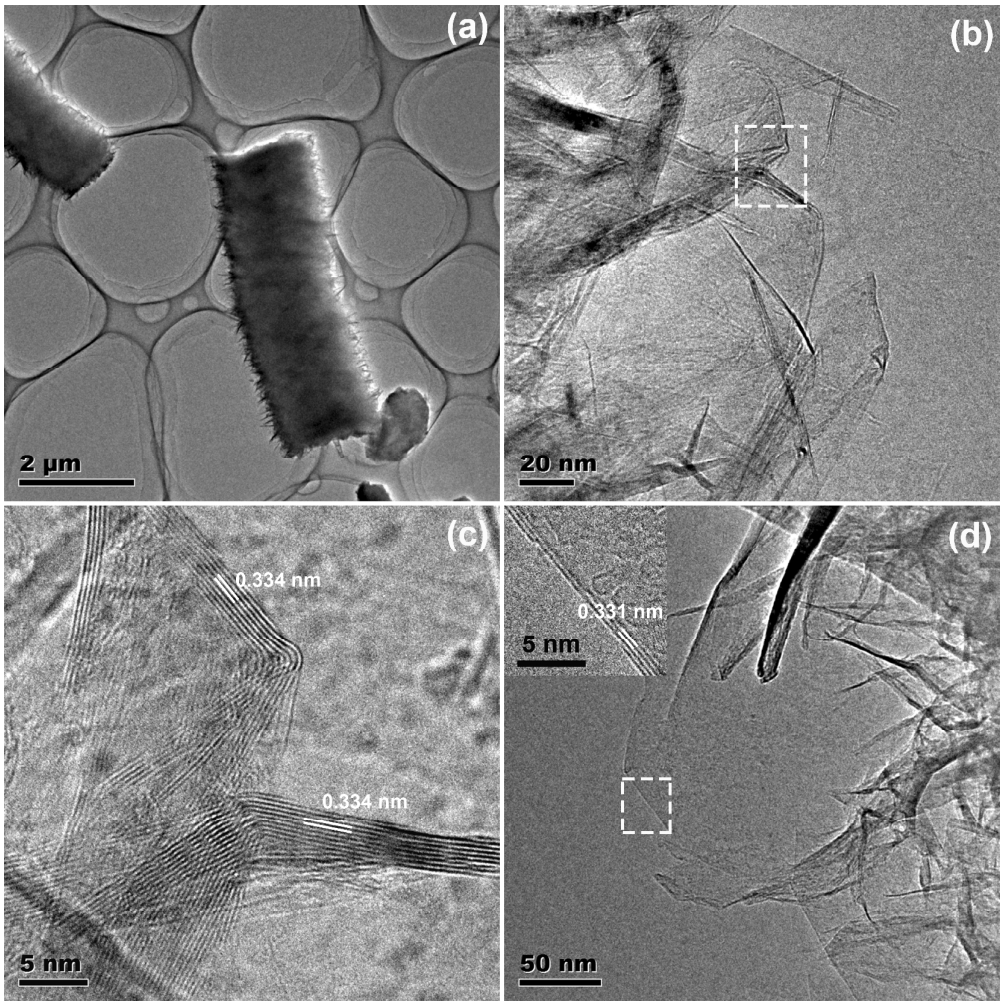

Fig. 4

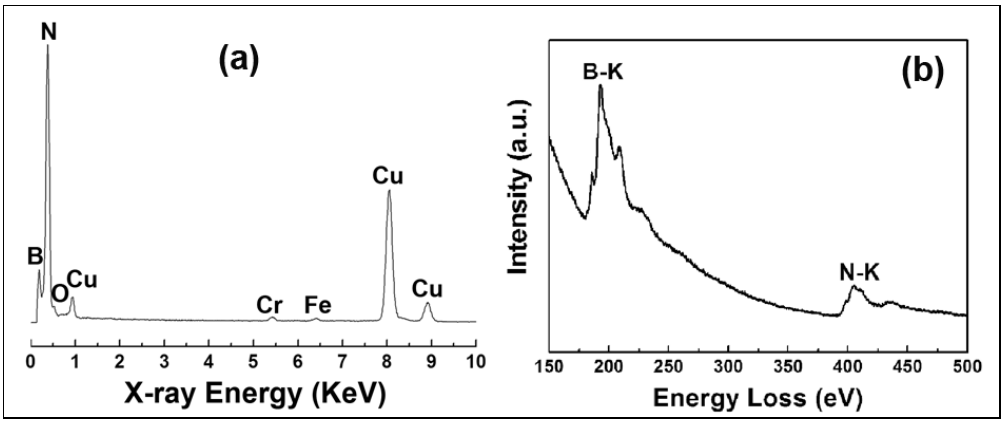

Fig. 5

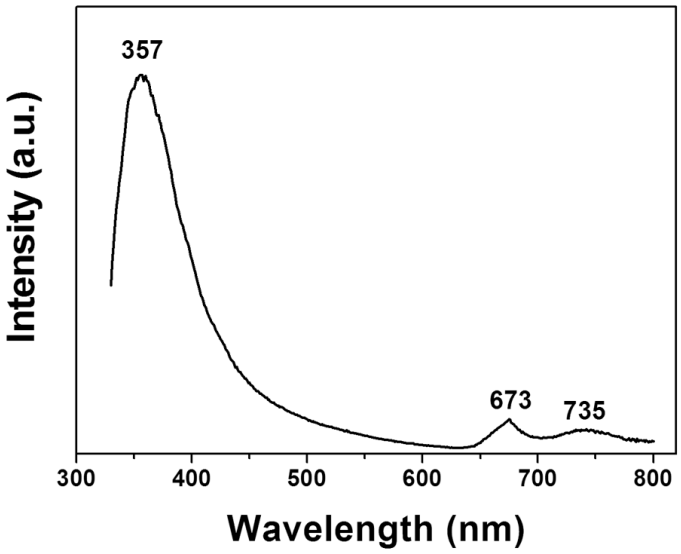

Fig. 6

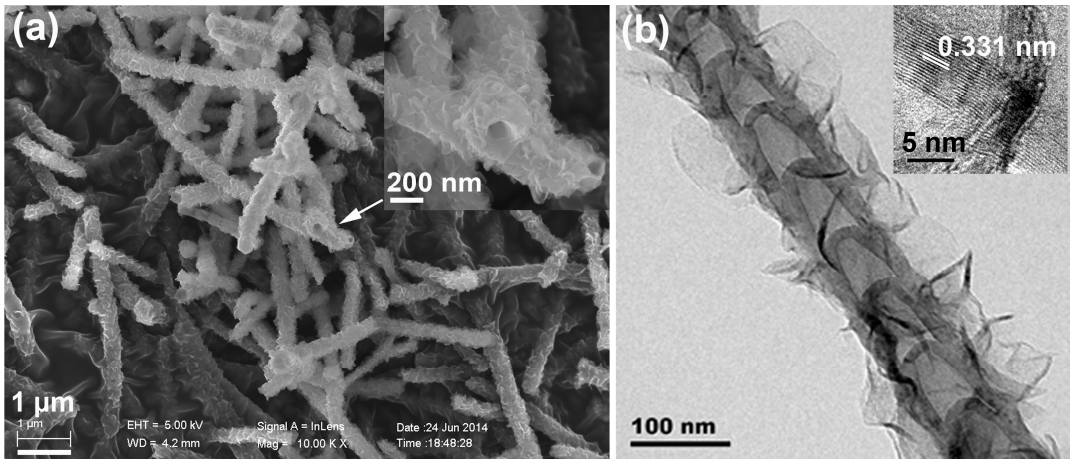

Fig. 7

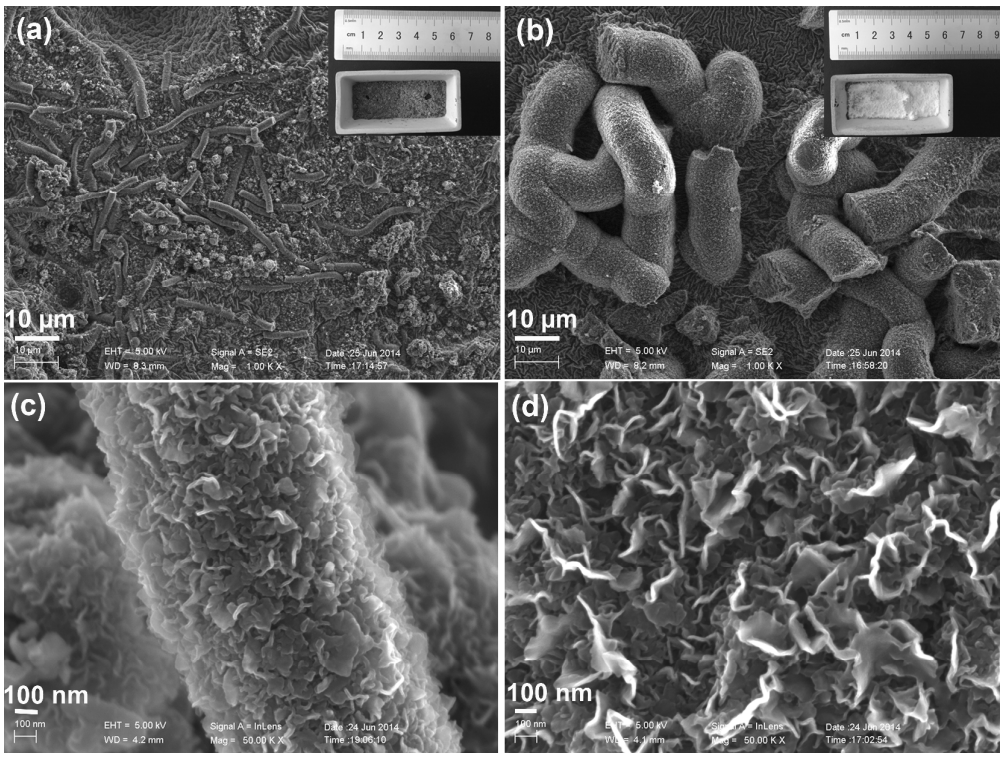

Fig. 8

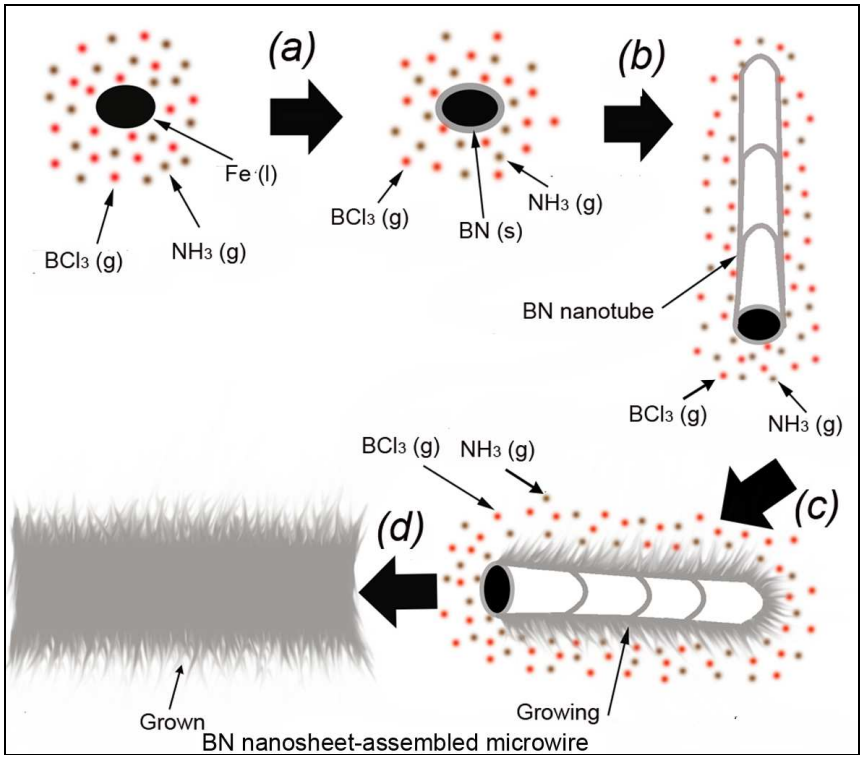

Table of contents

Boron nitride (BN) nanosheet-assembled microwires were successfully synthesized in large scale and with high purity via an efficient method.